

TRANSFER FUNCTION CHARACTERISTICS OF SUPER RESOLVING SYSTEMS

Tom D. Milster and Craig H. Curtis

Optical Sciences Center, University of Arizona, Tucson, Arizona 85721
(602) 621-8280ABSTRACT

Signal quality in an optical storage device greatly depends on the optical system transfer function used to write and read data patterns. The problem is similar to analysis of scanning optical microscopes. Hopkins (1) and Braat (2) have analyzed write-once-read-many (WORM) optical data storage devices. In this paper, we discuss transfer-function analysis of magneto-optic (MO) data storage devices with respect to improving transfer-function characteristics. Several authors (3)(4)(5) have described improving the transfer function as *super resolution*. However, none have thoroughly analyzed the MO optical system and effects of the medium. In our development, we discuss both the optical system transfer function and effects of the medium.

1. INTRODUCTION

An unfolded magneto-optic (MO) readout optical system is illustrated in Figure 1. Only one detector path is shown. $P_1(\sigma)$ represents the objective-lens aperture. $D(r_d)$ is the disk plane. A collection lens is shown following reflection from the medium. A second aperture, $P_2(\sigma)$, is associated with the collection lens. For most MO systems, the collection lens is a mirror image of the objective lens. The beam then passes through the partially polarizing beam splitter (PPBS) and a half-wave plate. The detector lens focuses the beam onto a detector that exhibits a responsivity as a function of position given by $R(r_d)$. For simplicity, we model $R(r_d)$ as a binary 1/0 (on/off) function. A polarizing beam splitter is placed after the detector lens to provide a complimentary optical path for the second detector.

MO read-back optics can be considered as either nonconfocal or confocal scanning optical microscopes. Nonconfocal systems collect all of the energy on the detectors, that is, $R(r_d) = 1$. Confocal systems place pinholes in detector planes. Pinholes pass only the central portion of the spot on each detector. The effect of each pinhole can be modeled as $R(r_d) = 1$ inside the pinhole and $R(r_d) = 0$ outside the pinhole.

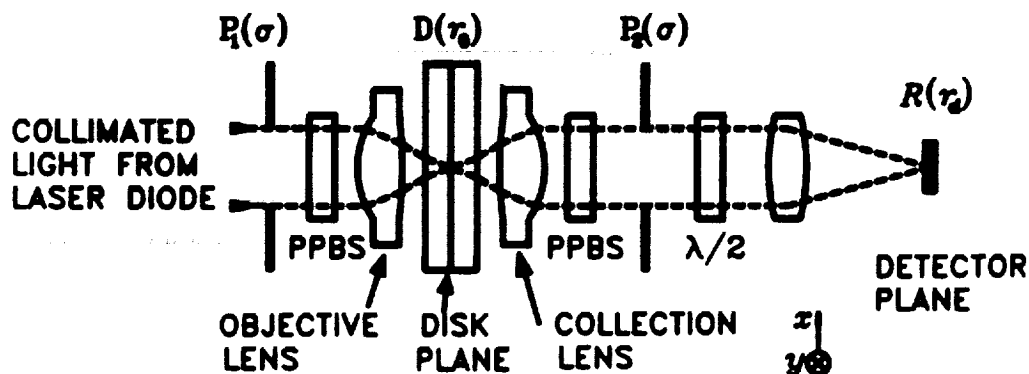


Figure 1. Unfolded MO detection system for one detector path.

detector planes. Pinholes pass only the central portion of the spot on each detector. The effect of each pinhole can be modeled as $R(r_s) = 1$ inside the pinhole and $R(r_s) = 0$ outside the pinhole.

In a separate paper (6), we have derived an expression for the signal current, i_{sig} as a function of scan position, r_s , that is given by

$$i_{sig}(r_s) = \int \int C(v;v') M(v;v') \exp\{-2\pi j(v - v') \cdot r_s\} dv dv', [1]$$

where $C(v;v')$ is the optical transfer function and $M(v;v')$ is the medium function described by

$$M(v;v') = Q(v)V^*(-v') + Q^*(-v')V(v), [2]$$

$Q(v)$ is proportional to the Fourier transform of the multiplication of the Kerr signal and the reflectivity. $V(v)$ is the Fourier transform of the reflectivity. In most MO systems, the reflectivity does not vary across the medium except as a phase perturbation in the x direction due to the presence of grooves. With constant reflectivity, $V(v)$ becomes $V(v) = \delta(v)$. If we assume line objects with frequency components in the y direction and $v_x = 0$ and $v_x' = 0$, $M(v;v')$ is only defined along the $v_y = 0$ and $v_y' = 0$ axes.

We illustrate the calculation of $i_{sig}(y)$ in Figure 2. A typical $C(v;v')$ contour is sketched that exhibits symmetry about the v_x and v_x' axes. Interaction with $C(v;v')$ is simplified due to the structure of $M(v;v')$. From Equation 2, the only overlap between $C(v;v')$ and $M(v;v')$ is along $v_y = 0$ and $v_y' = 0$ axes. After multiplication, a projection (integration) is performed along the v_x axis. Values of $i_{sig}(y)$ are calculated by taking the Fourier transform of the result along the v_x' axis.

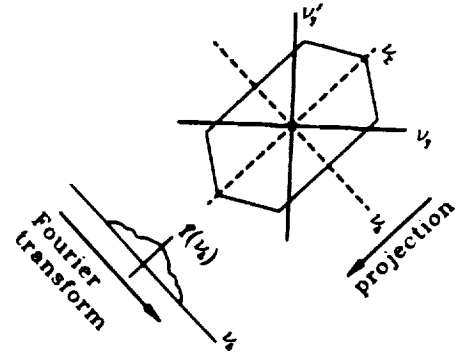


Figure 2. $i_{sig}(r_s)$ calculation. A typical $C(v;v')$ contour is shown.

3. Super-resolving optical systems

We now study several super-resolving optical layouts. The numerical aperture (NA) is 0.50 and $\lambda = 830$ nm. This results in a cutoff frequency, v_c of $NA/\lambda \approx 600$ lines/mm. Gaussian beam width for the overfill on $P_1(\sigma)$ is such that the $1/e^2$ beam irradiance is located at 90% of the pupil radius. This results in an optimum peak irradiance at the medium and power throughput as defined by Haskal (7). Optical layouts we consider include variations of $P_1(\sigma)$, $P_2(\sigma)$, and $R(r_s)$. Due to the nature of $M(v;v')$, we only display $C(v;v')$ along the $v_y' = 0$ axis. Also, transfer functions are normalized to their peak values, which results in a comparison of relative contrast values.

An example of our analysis is shown in Figure 3. A central obscuration is used to block a width s of $P_2(\sigma)$. Both nonconfocal (curves B1, C1, and D1) and confocal (curves B2, C2, and D2) cases are shown. For reference, curve A is the nonconfocal configuration using an open aperture for $P_2(\sigma)$. Curves B, C, and D correspond to $s/D = 0.25, 0.50,$ and $0.75,$ respectively. The frequency cutoff for all curves in Figure 3 is $2v_c$. For both the confocal and nonconfocal cases, a conservative obscuration width of 25% significantly improves the high-frequency response of the system without serious degradation at low frequencies. As s increases, high-frequency response improves at the cost of low-frequency response. Above 50% obscuration width, the confocal case does not significantly improve the transfer function.

Several super-resolving MO systems have been described in the literature. A system described by Yamanaka, Hirose, and Kubota (3) uses a prism arrangement to split and separate the Gaussian irradiance pattern on $P_1(\sigma)$. This distributes more power in the side lobes of the spot distribution on the medium. The spot is imaged onto a slit that is used to pass only the central lobe onto the detector. In Figure 4, curve A displays the nonconfocal configuration with $s/D = 0$ and the detector slit width, τ , completely open. This corresponds to curve A in Figure 3. Curve B

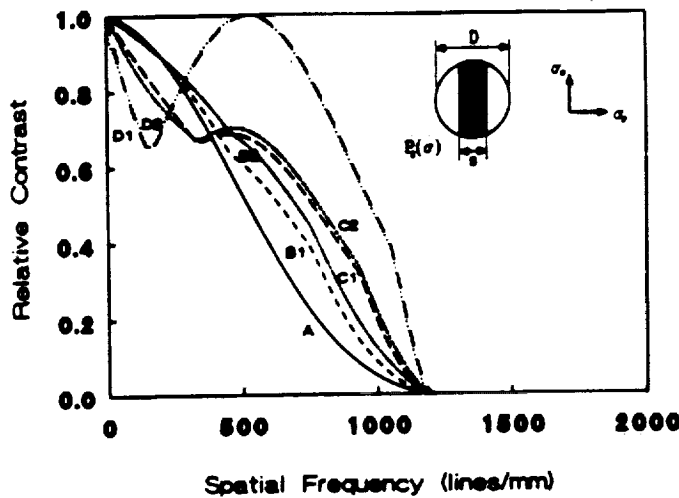


Figure 3. Transfer functions with rectangular obscurations in $P_2(\sigma)$.

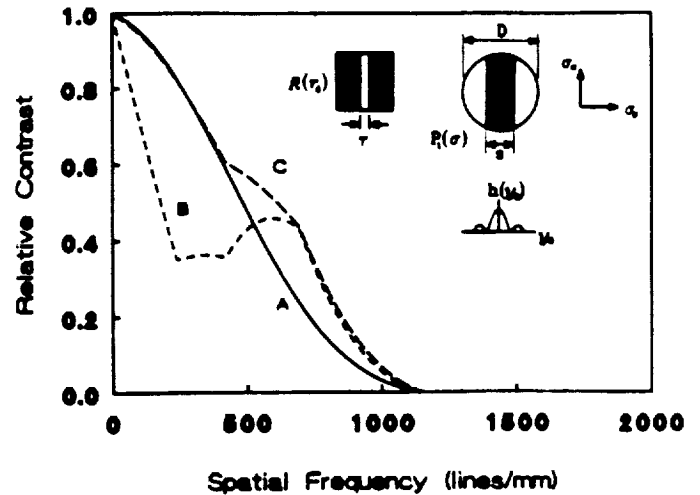


Figure 4. Transfer functions with rectangular obscurations in $P_1(\sigma)$.

corresponds to the case where $s/D = 20\%$ and τ is completely open. Even though the high-frequency response is moderately improved, the low-frequency response is severely degraded. Curve C corresponds to the case where $s/D = 20\%$ and τ is adjusted to pass only the central lobe to the detector. A significant improvement is obtained in high-frequency response while negligibly affecting low-frequency response.

It is worthwhile to compare curves from Figures 3 and 4. In Figure 3, the central obscuration is the collection optics, which decreases total power on the detectors. In Figure 4, the obscuration is in the illumination optics. This affects power throughput from laser to disk, which must be as high as possible in order to write data at high data rates. Transfer-function characteristics are similar for curve C of Figure 4 and curve B2 of Figure 3, so there appears to be no inherent advantage to placing the obscuration in the illumination optics.

Two other super resolving systems have been discussed. In the Suhara and Nishihara design of an integrated-optic CD disk pickup (4), super resolution improved readout performance. Another interesting system was proposed by Fukumoto et al. (5), in which the medium is self masking. A moderate improvement in the transfer function is observed in the mid-frequency range, and a significant improvement is observed in the high-frequency region. Other types of super resolving systems may be constructed from various apertures in $P_1(\sigma)$ and $P_2(\sigma)$. Aperture types include pinholes, annular rings, or slits. A more complete catalog of our results is found in Reference 6.

It is desirable to have a sharp edge response in MO readout. The edge response of the system can be found by applying procedures outlined in Figure 2. We first find $M(v, v')$ by a Fourier transform of $a(y_0) = \text{step}(y_0)$. We then multiply by a transfer function and inverse Fourier transform. Edge responses of several systems are shown in Figure 5. Curve A corresponds to the reference system where $P_1(\sigma)$ and $P_2(\sigma)$ are unobstructed and $R(r_d) = 1$ (nonconfocal). Curves B and C correspond to systems with shading bands of 25% and 50%, respectively, in the collection optics and $R(r_d) = 1$. A significant improvement in edge slope is observed for curve C. However, a ringing is observed as the shading band width increases. Curve D is the simulated response from Suhara's and Nishihara's waveguide coupler with $R(r_d) = \delta(r_d)$. No significant advantage of this system is observed. Curve E is the Fukumoto et al. system with an open $P_2(\sigma)$ and $R(r_d) = 1$. A smooth edge response with a steep slope is observed. Not shown is the Fukumoto et al. system with shading bands in the collection aperture, in which we have observed minimal increase in edge slope and noticeable increase in ringing.

Figure 6 displays how well two closely spaced bits are resolved. Two bits $1.56 \mu\text{m}$ long are separated by $0.52 \mu\text{m}$. Curve A represents the bits on the disk plane. Curve B is the reference system response with an open $P_2(\sigma)$ and $R(r_d) = 1$. A significant improvement is observed when compared to curve B. Curve D corresponds to a shading band of 50% in the collection optics and $R(r_d) = 1$. The dip in the detector current between the two bits is

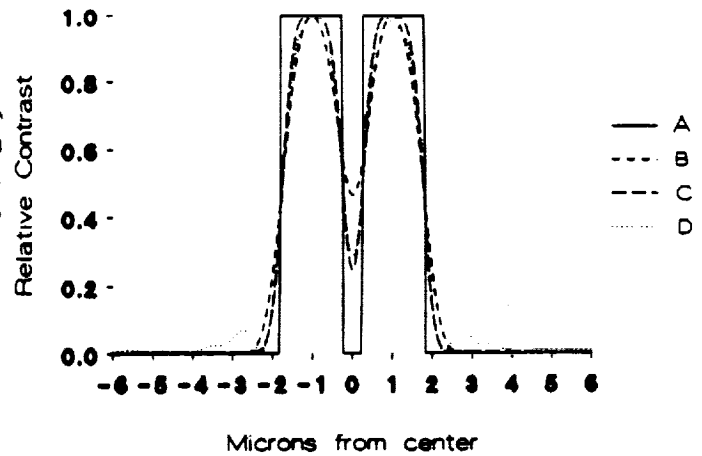
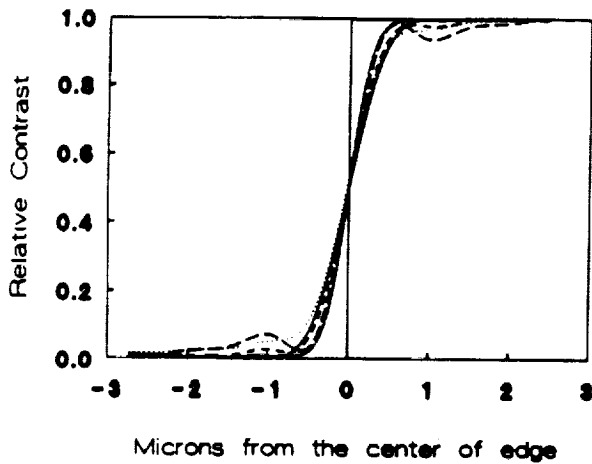


Figure 5. Edge responses for various super-resolving systems.

Figure 6. Two-point resolution of several systems.

comparable to the Fukumoto et al. system. However, the ringing observed in the edge response of Figure 5 exhibits itself as artifacts approximately ± 2.5 to $4.0 \mu\text{m}$ from the center of the pattern. Also, a slight disfiguring of the peak signal is observed.

4. Conclusions

We compared transfer functions of several super resolving MO data storage systems. We found that significant improvement can be obtained in several cases. Of the systems studied, the Fukumoto et al. system with an annular aperture for the collection optics gave the best edge response. In our analysis, we neglected effects of noise in the system. This is an active area in our research group, and we hope to augment our transfer-function analysis with noise studies in a later publication.

5. Acknowledgements

This work was supported by the Optical Data Storage Center. C. Curtis is supported by a fellowship under the Graduate Assistance in Areas of National Need (GAANN) Program.

6. References

1. H.H. Hopkins, "Diffraction theory of laser read-out systems for optical video disks," *JOSA A*, 22, p. 4 (1979).
2. J. Braat, "Optics of recording and read-out in optical disk systems," *Japanese Journal of Applied Physics*, 28, Supplement 28-3 pp. 103-108 (1989).
3. Y. Yamanaka, Y. Hirose and K. Kubota, "High density optical recording by superresolution," *Japanese Journal of Applied Physics*, 28, Supplement 28-3, pp. 197-200 (1989).
4. T. Suhara and H. Nishihara, "Possibility of super-resolution readout in integrated-optic disc pickup," Technical Digest of the International Symposium on Optical Memory, 1989, Kobe, Japan, September 26-28, pp. 97-98.
5. A. Fukumoto, et al., "Super resolution in a magneto-optical disk with an active mask," *SPIE Proceedings on Optical Data Storage*, 1499, pp. 216-225 (1991).
6. T.D. Milster and C.H. Curtis, "Analysis of super resolution in magneto-optic data storage devices," submitted for publication in *Applied Optics*.
7. H.M. Haskal, "Laser recording with truncated Gaussian beams," *Appl. Opt.*, vol 18, no. 13, pp. 2143-2146 (1979).

APPENDIX H

